The Crystal Structure of Fe_4S_4 Quinolinate Synthase Unravels an Enzymatic Dehydration Mechanism That Uses Tyrosine and a Hydrolase-Type Triad

Mickaël V. Cherrier,[†,‡] Alice Chan,[§] Claudine Darnault,[†] Debora Reichmann,[§] Patricia Amara,[†] Sandrine Ollagnier de Choudens,*,[§] and Juan C. Fontecilla-Camps*,[†]

[†]Metalloproteins Unit, Institut de Biologie Structurale, Commissariat à l'Energie Atomique—Centre National de la Recherche Scientifique, Université Grenoble-Alpes, 6 rue Jules Horowitz, 38000 Grenoble, France

[‡]UMR 5086, BMSSI, CNRS, Université Lyon 1, Institut de Biologie et Chimie des Protéines, 7 passage du Vercors, F-69367 Lyon, France

[§]Université Grenoble-Alpes, iRTSV-LCBM-Biocatalyse; CNRS, IRTSV-LCBM-Biocatalyse; CEA, iRTSV-LCBM-Biocatalyse, 38000 Grenoble, France

ⓢ *Supporting Information*

ABSTRACT: Quinolinate synthase (NadA) is a Fe_4S_4 cluster-containing dehydrating enzyme involved in the synthesis of quinolinic acid (QA), the universal precursor of the essential nicotinamide adenine dinucleotide (NAD) coenzyme. A previously determined apo NadA crystal structure revealed the binding of one substrate analog, providing partial mechanistic information. Here, we report on the holo X-ray structure of NadA. The presence of the Fe_4S_4 cluster generates an internal tunnel and a cavity in which we have docked the last precursor to be dehydrated to form QA. We find that the only suitably placed residue to initiate this process is the conserved Tyr21. Furthermore, Tyr21 is close to a conserved Thr-His-Glu triad reminiscent of those found in proteases and other hydrolases. Our mutagenesis data show that all of these residues are essential for activity and strongly suggest that Tyr21 deprotonation, to form the reactive nucleophilic phenoxide anion, is mediated by the triad. NadA displays a dehydration mechanism significantly different from the one found in archetypical dehydratases such as aconitase, which use a serine residue deprotonated by an oxyanion hole. The X-ray structure of NadA will help us unveil its catalytic mechanism, the last step in the understanding of NAD biosynthesis.

Biosynthesis of nicotinamide adenine dinucleotide (NAD), an essential and ubiquitous cofactor in biology, involves the formation of quinolinic acid (QA) in all living organisms.[1] QA is generated in most prokaryotes from L-aspartate and dihydroxyacetone phosphate (DHAP) through the concerted action of two enzymes, the L-aspartate oxidase NadB and the quinolinate synthase NadA.[2] Although the oxidation of L-aspartate to iminoaspartate (IA) catalyzed by NadB and the reactions from QA to NAD have been well characterized, the condensation of IA and DHAP to form QA, catalyzed by NadA, is still poorly understood at the molecular level[2] (Figure 1). *In vitro* studies demonstrated that in all systems studied so far NadA contains an oxygen-sensitive Fe_4S_4 cluster essential for

activity.[3−5] NadA is functionally and structurally similar to the citric acid cycle enzyme aconitase, i.e., both catalyze a dehydration process and coordinate a Fe_4S_4 cluster with only three cysteine protein ligands, which in NadA are organized in a $CX_{86−112}CX_{86−99}C$ motif.[5−7] Consequently, it was suggested that the unique iron site of the NadA Fe_4S_4 cluster (Fe_u) should also be directly involved in dehydration steps, acting as a Lewis acid. Partial mechanistic information has been obtained from the two available crystal structures of NadA,[8,9] which correspond to the inactive apo form of the enzyme. These structures reveal a common fold with two other Fe_4S_4 enzymes, IspH[10] and Dph2,[11] where the cluster is involved in redox reactions. To gain insight into the reaction catalyzed by NadA, we have determined the 1.65 Å resolution crystal structure of the active, Fe_4S_4-bound NadA from *Thermotoga maritima* (holo *Tm*NadA).

Initially grown holo recombinant wild-type *Tm*NadA crystals could not be used to determine its X-ray structure. Subsequently, two holo *Tm*NadA proteins, containing purposely engineered K219R and K280R mutations were produced. Only the former mutant, along with a His tag added at the protein N-terminus to facilitate purification, yielded a cluster of polycrystalline material (see Figures S1 and S2 for details). A fragment from this cluster was used to collect data at the European Synchrotron Radiation Facility (ESRF). The structure of *Tm*NadA K219R was subsequently solved by molecular replacement and refined at 1.65 Å resolution (Table S1 and Figure S1C). Examination of the crystal packing revealed the central role played by both the K219R mutation and, rather unexpectedly, the His tag (Figure S2). The holo *Tm*NadA K219R mutant exhibits biochemical (Fe and S content) and spectroscopic properties as the wild-type protein and displays both *in vivo* and *in vitro* NadA activity (Figure S3).

The presence of the natural Fe_4S_4 prosthetic group (Figure 2) in *Tm*NadA K219R reorganizes the interaction of the three protein domains relative to the apo malate-bound *Pyrococcus*
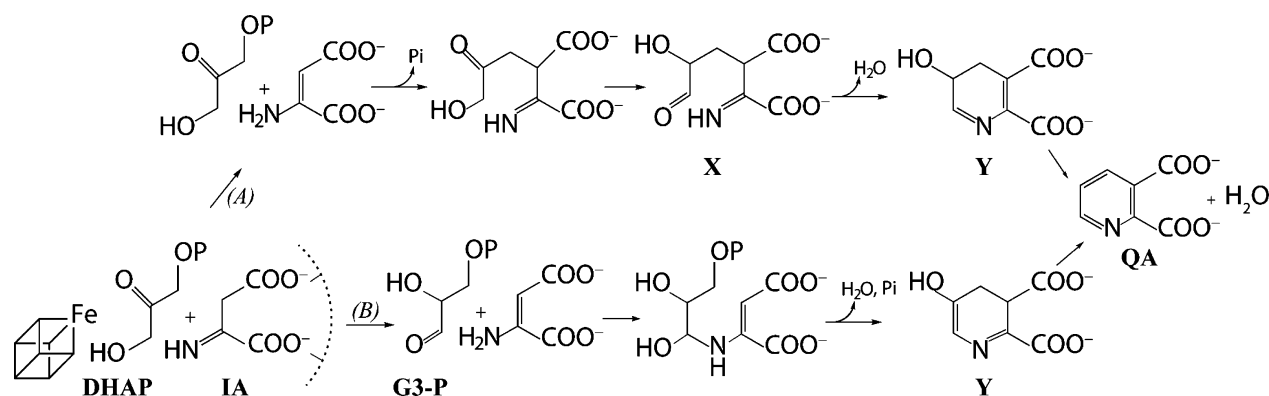
Figure 1. Previously proposed catalytic mechanisms for the synthesis of quinolinate from IA and DHAP by (A) Sakuraba et al.[8] and (B) Begley et al.[2] X = 2-imino, 3-carboxy, 5-hydroxy, 6-oxo hexanoic acid. Y = 5-hydroxy-4,5-dihydroquinolate. Fe_4S_4 cluster, which is essential for catalysis, is shown here, before the first step of each mechanism, at interacting distance from DHAP as suggested in ref 12. Malate-based[8] postulated interactions of IA with the protein (depicted as a semicircle in dashed lines) are also indicated.
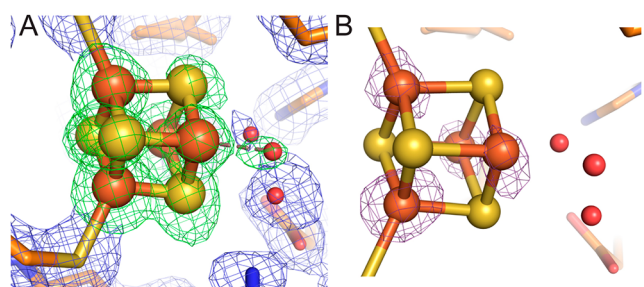

Figure 2. (A) Omit $(F_o - F_c)$ electron density map (green mesh contoured at 3σ) at the Fe_4S_4 cluster and its solvent ligand with its environment shown within its matching $(2F_o - F_c)$ map (blue mesh contoured at 1σ). Atom color codes: orange: Fe, yellow: S, red: H_xO, gold: C. Dashed line connects the unique Fe to the solvent molecule that completes its tetrahedral coordination. (B) Δ_{anom} electron density map contoured at 3σ calculated at the Fe_4S_4 cluster (X-ray data collected at $\lambda = 0.979$ Å). As expected, peaks are found at the Fe ions positions.

Figure 3. (A) (left) Structure of holo TmNadA K219R. Three domains (green, purple and gold) define a tunnel that connects the Fe_4S_4 cluster to the molecular surface; (right) section through the long tunnel of the structure rotated by 90° about the vertical axis. Fe_4S_4 cluster is displayed as balls and sticks. (B) Section of the apo PhNadA structure[8] (same orientation as rotated in B). Note the absence of the tunnel that is found in holo TmNadA. Bound malate is displayed as balls and sticks.

horikoshii NadA (*Ph*NadA),[8] (Figure S4). As expected, the binding of the Fe_4S_4 cluster also results in the ordering of the Cys-bearing interdomain stretches of TmNadA K219R. The interdomain interactions in the holo structure generate a long tunnel connecting the Fe_4S_4 cluster to the molecular surface (Figure 3A). The mobility of domain III relative to domains I and II, as indicated by the *Ph*NadA structure (Figure S4), may finely modulate the size and shape of the tunnel when substrate is bound. Indeed, a comparison between apo *Ph*NadA and our structure shows that binding of malate induces the collapse of the internal tunnel (Figure 3B). Although this conformational change may result from the absence of the Fe_4S_4 cluster it would make sense for the active enzyme to shield the unstable IA from the exterior.[13] A comparison of the interaction energies of domains I and II with domain III in our structure and *Ph*NadA indicates that a conformational change of the latter domain should not involve a significant relative energy change (Table S2).

Soriano et al.[9] have modeled the binding cavity of NadA from a combination of the apo *Ph* and *Pyrococcus furiosus* (*Pf*) X-ray NadA structures. Furthermore, they have placed substrates and the last QA precursor in their model. However, the modeled positions of some relevant amino acid side chains appear to be significantly different from their counterparts in the holo TmK219R NadA X-ray structure (not shown).
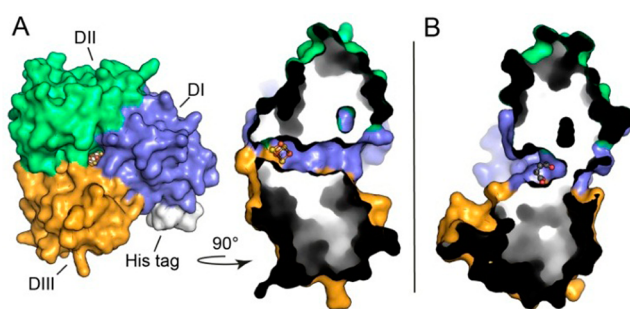
Conversely, the apo *Ph*NadA structure reported by Sakuraba et al.[8] defines the binding site of IA because the bound malate is analogous to this substrate. However, in the absence of the Fe_4S_4 cluster, the DHAP binding site, including the unique iron cluster site and essential functional amino acids, is undefined.

Besides a different orientation of domain III, the comparison of TmNadA K219R and PhNadA reveals changes at the malate-binding site. These include a 2.5 Å shift of the α-helix formed by residues 35−45 of domain I and a less extensive displacement of the loop containing Ser124 of domain II, both directed toward the carboxylate groups of the IA analog. These two localized conformational changes (Figure S5) were built into our holo TmNadA K219R structure using homology modeling. This allowed us to reproduce the binding of the COOH groups of the IA-derived fragment of the last QA precursor 5-hydroxy-4,5-dihydroquinolinate (5-OH-4,5-DHQA; Y in Figure 1) in the active site structure. Subsequently, a mechanistic study was initiated using two anchoring points to dock the precursor into the catalytic cavity of the above model (modeling details in Supporting Information, SI): (i) the two malate carboxylate groups positions and (ii) the expected direct interaction of the −OH group of the precursor with the unique Fe from the cluster (as determined for the −SH groups of the 4,5-dithiohydroxyphtalic acid (DTHPA) inhibitor).[12] Subsequently, the position of
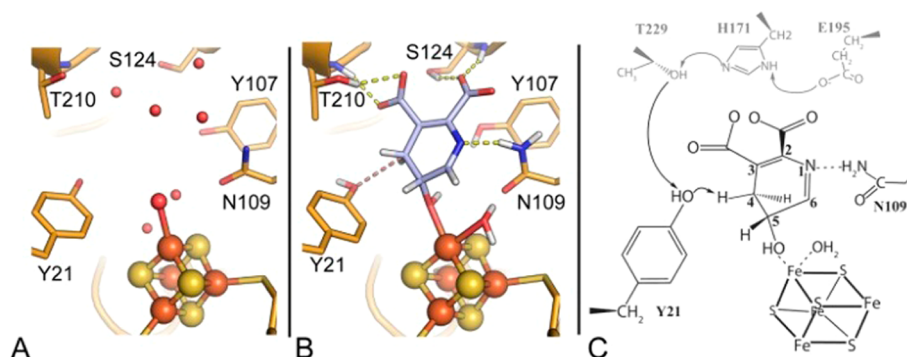
Figure 4. (A) View of the active site cavity of holo *Tm*NadA. (B) The most suitable 5-OH-4,5-DHQA (*R*) precursor of QA (carbon atoms in blue) docked in the NadA modified active site. Hydrogen bonds between the ligand and the protein are indicated in yellow; the possible attack of the H atom of C4 by Tyr21 is depicted in pink. (C) Schematic view of the active site of *Tm*NadA with the docked QA precursor, a modeled H_2O molecule bound to Fe_u, Tyr21, and Asn109, and the charge-relay system made of Thr229, His171, and Glu195. Arrows indicate proton abstractions.

residues interacting with the 5-OH-4,5-DHQA models was optimized. Among the possible isomers, we found that the C5-centered (*R*) model of the docked 5-OH-4,5-DHQA, with one of the two possible ring puckerings, satisfied the anchoring requirements. Furthermore, it provided a structural basis for catalysis (Figure 4). Indeed, in this conformation a suitable functional group, the −OH from Tyr21, is properly positioned to become the nucleophile that deprotonates C4, a step required in the dehydration of 5-OH-4,5-DHQA to form QA (Figures 1 and 4C). In the alternative orientation for the anchoring carboxylate groups, the potentially catalytic Tyr107 and Ser36 are too far from C4. Furthermore, their geometry is not appropriate for C4 proton abstraction, and there is no obvious way of generating a reactive alkoxide nucleophile from the hydroxyl group of either residue (not shown).

Incidentally, we noted that the long tunnel that connects the catalytic unique iron ion of the Fe_4S_4 cluster to the molecular surface collapses in our *Tm*NadA model in which (*R*) 5-OH-4,5-DHQA was docked (Figure S6). This suggests that substrate binding controls the opening and closure of the tunnel.

We have subsequently shown that Tyr21 plays a central functional role in NadA catalysis by mutating it to Phe in the *T. maritima* enzyme (see SI). Indeed, the *Tm*NadA Y21F mutant, which still coordinates a Fe_4S_4 cluster, displayed no detectable enzymatic activity (Table S3). This result was confirmed with the corresponding Y49F mutant of the more active *E. coli* NadA. In *Tm*NadA K219R the role of Tyr21 in the deprotonation of 5-OH-4,5-DHQA is further substantiated by its interaction with a charge-relay system composed of the strictly conserved residues Thr229, His171, and Glu195. This system, which is similar to the Ser-His-Asp catalytic triad typical of serine proteases and other hydrolases,[14] should favor the formation of a nucleophilic phenoxide anion at Tyr21 (which directly interacts with Thr229) (Figures 4C and 5). In order to test this hypothesis, triad mutants were generated in the *E. coli* NadA enzyme. They all display a drastically reduced activity showing that the triad residues are also crucial for catalysis (Table S3). The residual activity observed in these mutants is not due to impaired substrate binding because they all bind the DTHPA inhibitor like the wild type protein does (Figure S7).

Thr and Glu residues, rather than the classic Ser and Asp, are also used in other triads. For instance, Glu is found in the catalytic triad of acetylcholine esterase from *Torpedo californica* and Thr in the triad from asparaginases.[14] It should be noted
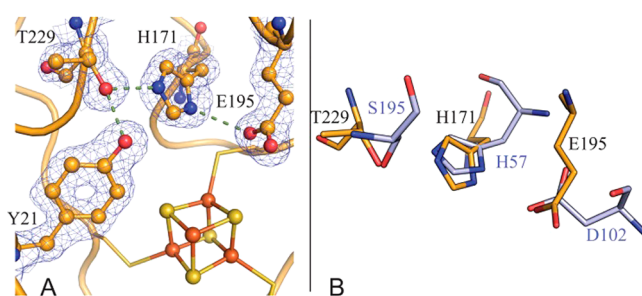

Figure 5. (A) Charge-relay triad (Thr229-His171-Glu195) and Tyr21, depicted with their matching $(2F_o−F_c)$ electron density map, at the NadA active site. (B) Superposition of our proposed Thr-His-Glu triad with the catalytic Ser-His-Asp triad of bovine trypsin (PDB code 4I8G).[15] The carbon atoms of *Tm*NadA and trypsin are shown as gold and light-blue sticks, respectively; blue: N, red: O.

that His171 also interacts with Cys168, a ligand of the Fe_4S_4 cluster. However, this interaction is not likely to play a determinant role in either Fe−S cluster biogenesis or stabilization because the corresponding H205F mutant coordinates a Fe_4S_4 cluster. In conclusion, the observed charge-relay triad is unprecedented and could not have been identified from previous NadA structural data or models derived from them.

Our results may be compared to those reported for aconitase, which is the archetypical enzyme for Fe_4S_4 cluster-based dehydration/hydration reactions.[16,17] The condensation of IA with DHAP to generate QA involves two dehydrations by NadA, but only the second one is mechanistically equivalent to the synthesis of aconitate from citrate. The first dehydration involves a carbinolamine intermediate, which results from the nucleophilic attack of either −NH2 or =NH2+ to the >C=O group of glyceraldehyde 3-phosphate (G3-P) resulting from the tautomerization of DHAP or to the >C=O group of the tautomerized **X** product (Figure 1). This will depend on which of the previously proposed two mechanisms (Figure 1) is assumed to be the correct one. The reactivity of the >C=O group with the nucleophile will be a function of its electrophilicity. An interaction of the unique Fe ion from the cluster with >C=O would make this group more electrophile and will favor the reaction. The *Tm*NadA K219R structure does not allow us to provide a detailed model for the stereo-chemistry of this reaction, but it is certainly compatible with a close (<2.0 Å) terminal >C=O···Fe_u interaction. The

nucleophilic attack has to take place on an aldehydic terminal >C=O to produce the appropriate intermediate in QA synthesis (Figure 1). The second dehydration step, that of 5-OH-4,5-DHQA to QA, requires the deprotonation of its C4 followed by elimination as water of the C5-linked −OH group of the Fe_u-bound precursor. This reaction is likely to be very similar to the dehydration of citrate to yield aconitate because it also generates a >C=C< bond, with the additional advantage of resulting in aromatization. The Fe_u in the *Tm*NadA K219R structure appears to have a more extensive coordination than its counterpart in ligand-free aconitase. However, there is a well-defined, most probably H_2O/OH^-, ligand that completes the tetrahedral coordination of Fe_u like OH^- does in that enzyme[16] (Figures 2 and 4A and SI).

As mentioned above, our structural and functional data indicate that the only plausible candidate for the nucleophile that deprotonates 5-OH-4,5-DHQA in *Tm*NadA is Tyr21. When compared to aconitase there are two major differences: the nature of the alkoxide-bearing residue, which is Ser in that enzyme, and the way the alkoxide is generated. In aconitase, the active site Ser642 accepts short H-bonds from an oxyanion hole, formed by the main chain amide and the Nε atom from Arg644, that lower its pK_a enough to facilitate its deprotonation upon citrate or isocitrate binding.[16−18] Conversely, as discussed above, in NadA the deprotonation of Tyr21 is likely to be unusually carried out by a charge-relay system similar to typical catalytic triads of the hydrolase family (Figures 4C and 5). This process represents a remarkable convergent use of such triad.[19]

In summary, holo NadA displays a combination of remarkable features that, besides the dehydration mechanism described above, includes a long tunnel that connects the catalytic unique iron ion of the Fe_4S_4 cluster with the molecular surface and collapses upon substrate binding. Our efforts will be now concentrated in generating structures of NadA with substrate analogs, inhibitors, and NadA variants in order to get further insights into the NadA catalytic mechanism and design potential antibacterial agents. Indeed, NadA constitutes a therapeutic target in some pathogens such as *Mycobacterium leprae* and *Helicobacter pylori*.

■ ASSOCIATED CONTENT

Ⓢ Supporting Information

Experimental details and crystallographic data. The structure has been deposited in the Protein Data Bank as entry 4P3X. This material is available free of charge via the Internet at http://pubs.acs.org.

■ AUTHOR INFORMATION

Corresponding Authors
juan.fontecilla@ibs.fr
sandrine.ollagnier@cea.fr

Notes
The authors declare no competing financial interest.

■ ACKNOWLEDGMENTS

■ REFERENCES

(1) Frey, P.; Hegeman, A. D. *Enzymatic Reaction Mechanisms*; Oxford University Press: New York, 2007.
(2) Begley, T. P.; Kinsland, C.; Mehl, R. A.; Osterman, A.; Dorrestein, P. *Vitam. Horm.* **2001**, *61*, 103.
(3) Ollagnier-de Choudens, S.; Loiseau, L.; Sanakis, Y.; Barras, F.; Fontecave, M. *FEBS Lett.* **2005**, *579*, 3737.
(4) Cicchillo, R. M.; Tu, L.; Stromberg, J. A.; Hoffart, L. M.; Krebs, C.; Booker, S. J. *J. Am. Chem. Soc.* **2005**, *127*, 7310.
(5) Marinoni, I.; Nonnis, S.; Monteferrante, C.; Heathcote, P.; Hartig, E.; Bottger, L. H.; Trautwein, A. X.; Negri, A.; Albertini, A. M.; Tedeschi, G. *FEBS J.* **2008**, *275*, 5090.
(6) Rousset, C.; Fontecave, M.; Ollagnier de Choudens, S. *FEBS Lett.* **2008**, *582*, 2937.
(7) Saunders, A. H.; Griffiths, A. E.; Lee, K. H.; Cicchillo, R. M.; Tu, L.; Stromberg, J. A.; Krebs, C.; Booker, S. J. *Biochemistry* **2008**, *47*, 10999.
(8) Sakuraba, H.; Tsuge, H.; Yoneda, K.; Katunuma, N.; Ohshima, T. *J. Biol. Chem.* **2005**, *280*, 26645.
(9) Soriano, E. V.; Zhang, Y.; Colabroy, K. L.; Sanders, J. M.; Settembre, E. C.; Dorrestein, P. C.; Begley, T. P.; Ealick, S. E. *Acta Crystallogr., Sect. D: Biol. Crystallogr.* **2013**, *69*, 1685.
(10) Grawert, T.; Span, I.; Eisenreich, W.; Rohdich, F.; Eppinger, J.; Bacher, A.; Groll, M. *Proc. Natl. Acad. Sci. U S A* **2010**, *107*, 1077.
(11) Zhang, Y.; Zhu, X.; Torelli, A. T.; Lee, M.; Dzikovski, B.; Koralewski, R. M.; Wang, E.; Freed, J.; Krebs, C.; Ealick, S. E.; Lin, H. *Nature* **2010**, *465*, 891.
(12) Chan, A.; Clemancey, M.; Mouesca, J. M.; Amara, P.; Hamelin, O.; Latour, J. M.; Ollagnier de Choudens, S. *Angew. Chem., Int. Ed. Engl.* **2012**, *51*, 7711.
(13) Rizzi, M.; Schindelin, H. *Curr. Opin. Struct. Biol.* **2002**, *12*, 709.
(14) Dodson, G.; Wlodawer, A. *Trends Biochem. Sci.* **1998**, *23*, 347.
(15) Liebschner, D.; Dauter, M.; Brzuszkiewicz, A.; Dauter, Z. *Acta Crystallogr., Sect. D: Biol. Crystallogr.* **2013**, *69*, 1447.
(16) Beinert, H.; Kennedy, M. C.; Stout, C. D. *Chem. Rev.* **1996**, *96*, 2335.
(17) Lloyd, S. J.; Lauble, H.; Prasad, G. S.; Stout, C. D. *Protein Sci.* **1999**, *8*, 2655.
(18) Lauble, H.; Kennedy, M. C.; Beinert, H.; Stout, C. D. *Biochemistry* **1992**, *31*, 2735.
(19) Gutteridge, A.; Thornton, J. M. *Trends Biochem. Sci.* **2005**, *30*, 622.